Role of Germanium on the Nucleation and Growth of Zeolite A from Clear Solutions As Studied by in Situ Small-Angle X-ray Scattering, Wide-Angle X-ray Scattering, and Dynamic Light...

ARTICLE *in* THE JOURNAL OF PHYSICAL CHEMISTRY C · OCTOBER 2009

Impact Factor: 4.77 · DOI: 10.1021/jp907542a · Source: OAI

Role of Germanium on the Nucleation and Growth of Zeolite A from Clear Solutions As Studied by in Situ Small-Angle X-ray Scattering, Wide-Angle X-ray Scattering, and Dynamic Light Scattering

Matthew G. O'Brien,*,†,‡ Andrew M. Beale,§ Bonny W. M. Kuipers,|| Ben H. Erné,|| Dewi W. Lewis,† and C. Richard A. Catlow†

Department of Chemistry, Christopher Ingold Laboratories, University College London, 20 Gordon Street, London WC1H 0AJ, United Kingdom, and Inorganic Chemistry and Catalysis, Department of Chemistry, Debye Institute for Nanomaterials Science, Utrecht University, Sorbonnelaan 16, 3584 CA, and Van't Hoff Laboratory for Physical and Colloid Chemistry, Debye Institute for Nanomaterials Science, Utrecht University, Padualaan 8, 3584 CH, Utrecht, The Netherlands

Received: August 5, 2009; Revised Manuscript Received: September 14, 2009

Understanding the formation processes of zeolites is essential if a more "rational" design principle, leading to more catalytically useful materials, is to be achieved. Optically clear "model" solutions allow for significant insight, while systematic variation of selected experimental conditions can reveal additional detail of these complex processes. In this work we have studied the synthesis of zeolite A from clear solutions and compared the effect of isomorphous germanium substitution on this process. To follow the entire process, a combination of in situ time-resolved small-angle X-ray scattering, wide-angle X-ray scattering, and dynamic light scattering was used. These techniques indicate a mechanism similar to that observed for silicalite-1 with the formation of amorphous nanoparticles that become increasingly stable until growth continues by addition to aggregates. Additionally, by comparison between the unsubstituted and germanium-substituted materials, we have identified the effect of metal substitution and have shown how it has a significant influence over the entire formation process, from the formation and stabilization of the initial nanoparticles to the type and rate of crystallization and the final crystal morphology. This study therefore demonstrates the importance of metal substitution effects for controlling the rational design of zeolites and indicates that a greater understanding of these effects is required to fully understand these systems.

Introduction

The molecular selectivity and acidity of nanoporous zeolite materials has been used over the past few decades for chemical processes such as catalytic cracking and the methanol to olefin conversion.[1−5] However, due to mismatches between the pore structures required for specific chemical reactions and those available in the zeolites, the majority of these materials remain unexploited. Much time and effort has therefore been invested in attempting to develop "designer" materials in which the final structure of the pore system is both predicted and controlled, although owing to the highly complex nature of the hydrothermal reaction process, this objective is difficult to achieve.[6] Such prediction and control inherently requires a deep understanding of the synthesis process of such materials, and these have been subjected to numerous investigations over many years using a variety of both in situ and ex situ methods.[7,8]

Zeolites are most commonly crystallized from a gel containing the required ingredients; however, procedures for synthesis from optically clear solutions exist for a number of materials. These have the advantage of acting as simplified synthesis "models", allowing a more simple interpretation of data from, for example, nuclear magnetic resonance (NMR) and small-angle X-ray scattering (SAXS), and allowing the use of techniques such as dynamic light scattering (DLS) to provide more insight into the self-assembly process.[19,14] Of course, as the ultimate aim of research into zeolite synthesis is to understand this entire process (from the initial nanometer-sized nuclei through the intermediates and to the final micrometer-sized crystals), it is desirable to combine a number of these techniques to access all the required length scales, either in a single experiment or as a number of complementary in situ and/or ex situ experiments. A widely used example of this is the combination of small- and wide-angle X-ray scattering (SAXS and WAXS) in combination with DLS.[9−14]

Nevertheless, despite the wide availability of the techniques discussed above, there still remains considerable debate over the exact nature of the synthesis processes. This is due in part to the range of particles observed under different synthesis conditions, which then evolve differently during the formation of the final zeolite material.[7,8] For example, initial nuclei have been suggested to be both continuously produced and formed in a single event, while numerous larger species have been observed, ranging from 2 to over 100 nm.[15−20] Therefore, we also note that the exact processes involved in zeolite synthesis may depend on the specific system, and there may be no "unifying" mechanism. A detailed overview of the many mechanisms is given in the reviews by Cundy and Cox.[7,8] Here, however, we focus on the particular debate surrounding the nature and role of the nanosized (generally <6 nm) particles.

* To whom correspondence should be addressed. E-mail: M.G.Obrien@uu.nl.
† University College London.
‡ Current address: Inorganic Chemistry and Catalysis, Department of Chemistry, Debye Institute for Nanomaterials Science, Utrecht University.
§ Inorganic Chemistry and Catalysis, Department of Chemistry, Debye Institute for Nanomaterials Science, Utrecht University.
|| Van't Hoff Laboratory for Physical and Colloid Chemistry, Debye Institute for Nanomaterials Science, Utrecht University.

10.1021/jp907542a CCC: $40.75
Published on Web 10/02/2009

The existence of these particles has been well reported in the literature, particularly for silicalite-1 synthesis, and their existence is now widely accepted.[21,22] However, there are various interpretations of their exact nature and role in the formation process, which has resulted in three substantially different mechanisms.[21,22]

In the first mechanism, the particles are described as being amorphous and stable and do not participate in the growth processes, with formation of the final product occurring via monomer addition.[8,23] The second describes an active role of the still amorphous particles which aggregate (the process of which may be rate limiting) into larger materials which eventually convert in some manner to the final crystals.[24−27] The third process also proposes an aggregation pathway but also suggests that the aggregates possess either some medium-range order[28] or the actual zeolite structure from early on in the process.[29,30]

One way to gain more insight into the formation process and the significance of the nanoparticles is to systematically vary some of the synthesis parameters and observe the resulting effect. For zeolite systems the substitution of a tertiary metal ion into the framework must be considered a prime candidate, as substitution not only provides more catalytically interesting materials, but is also already known to influence the final zeolite product (and therefore by inference the growth process).[31−34] To date, however, there have been few clear solution studies on such systems, which is at least partly due to the difficulties in obtaining clear solutions with good substitution levels. Recently though, the insertion of Ge into silicalite-1 has been demonstrated and resulted in enhanced rates of formation as the Si/Ge ratio reached 15 and 25, although interestingly a decrease was then noted on further substitution.[10,11] Such enhancement effects are not surprising, as Ge is able to stabilize the acute T−O−T angles required in particular zeolite structural units, such as double four-membered rings (D4Rs), and can promote the formation of a number of unusual structures.[35−40] Indeed, recent mass spectroscopy studies of prenucleation silicate solutions have demonstrated the location of Ge within D4R structures, while D4Rs have been observed at a very early stage during the formation of zeolite A.[28,41]

To this end, we demonstrate here the first synthesis of optically clear Ge-substituted zeolite A at high substitution levels and compare this with the unsubstituted system using combined in situ SAXS/WAXS and complementary in situ DLS measurements. Initially we determine the formation process for zeolite A and then examine the specific effect of Ge on nanoparticle formation. We then examine the effect of Ge on the rest of the synthesis, including the crystallization process and the final crystalline products. Our study therefore demonstrates the important role of metal substitution on the entire formation and crystallization process of zeolites and demonstrates that a greater understanding of this will be required if we are to exercise control over the zeolite formation process and final product.

Experimental Section

Synthesis of Zeolite A and Substituted Zeolite A. Zeolite A was synthesized using a method similar to that of Mintova et al. but using tetramethylammonium silicate solution to prepare a clear solution.[42] Typically, to the required quantity of 16.9% tetramethylammonium silicate solution (Aldrich) was slowly added the corresponding molar equivalent of GeO_2 (Aldrich) powder while the mixing vessel was agitated, and the mixture was then stirred for 10−15 min. Upon dissolution, 25% tetramethylammonium hydroxide (TMAOH), water, and 10 M sodium hydroxide solution were added to the mixture. The solution was then aged (ca. 15 min), and then aluminum isopropoxide was added with stirring. The opaque solution was left to stand with occasional agitation for 2 h, during which time a clear solution was obtained. It was then filtered through 2 μm Whatman syringe filters prior to treatment by hydrothermal methods.

Ex Situ Measurements. ***X-ray Diffraction (XRD).*** XRD patterns of the final products were recorded using a Bruker D8 diffractometer in the Debye−Sherrer orientation using a 1 mm capillary. X-rays were generated from a copper source (1.540598 Å) with a secondary monochromator to remove any $K_{\alpha 2}$ and Cu K_β radiation and using a step size of $2\theta = 0.007°$. The Fullprof suite of programs was used to perform Le Bail fits.

Extended X-ray Adsorption Fine Structure (EXAFS). EXAFS measurements (Supporting Information Figure S1) were carried out at station 9.3 of the SRS at Daresbury Laboratories using a Si(220) double-crystal monochromator in transmission mode. Samples consisted of 40 mg of laboratory-prepared zeolite A pressed into 13 mm pellets. The data were then analyzed using the analysis suite available from Daresbury Laboratories, namely, EXCALIB, EXSPLINE, and EXCURV98.

Scanning Electron Microscopy (SEM). SEM images were taken using a JEOL JSM-6301F scanning microprobe, and energy-dispersive X-ray analysis (EDX) was performed using a Hitachi EDX 5570 fitted with an Oxford Instruments INCA analysis suite for data processing.

In Situ SAXS Measurements. ***Experimental Setup.*** Combined SAXS/WAXS measurements were carried out at station 6.2 of the Daresbury SRS using the angule-dispersive RAPID2 WAXS detector over an angle of $2\theta = 60°$ and a RAPID2 quadrant SAXS camera with lengths ranging from 1.3 to 3 m.[43] The unsubstituted zeolite A was recorded with an X-ray wavelength of 1.127 Å (11.000 keV) at a SAXS camera length of 3 m and 1.400 Å (8.856 keV) at 1.3 m ("short camera", Supporting Information Figure S2), whereas the Ge 5% and 15% substituted materials were recorded at 1.400 Å at 3 m ("long camera") and the 23%-substituted material was recorded at 1.400 Å at 1.3 m. Calibration of the SAXS detector was performed using the periodic standard wet rat tail collagen ($d = 670$ Å), while silicon was used for the wide-angle detector. We note that a "kink" in the raw data at high Q was observed; however, further analysis revealed this to be due to the quadrant detector response at high Q and not particle formation (Supporting Information Figure S3). Measurements were performed in a hydrothermal cell (0.5−2 mL volume) designed in-house (Supporting Information Figure S4) placed into a heating block mounted on the SAXS/WAXS sample stage and preset at the desired temperature of 90 °C. All measurements were started 2 min after insertion of the sample.

Data Analysis. The data were initially calibrated for beam decay, normalized, background subtracted, and converted to ASCII using OTOKO and in-house Matlab macros.[44] For convenience of comparison with the DLS data, the SAXS data in this work are plotted against d using the relation $q = 2\pi/d$, where q is the scattering vector and d is the distance between scatters.[45] The maximum intensity of the particle populations (labeled **I** and **II** in the discussion below) were then recorded throughout the reaction. Again from using the relation $q = 2\pi/d$, the diameter of **I** at maximum intensity can be initially estimated. However, as Aerts et al. have previously demonstrated, the calculation of the SAXS particle diameter directly from these maxima can result in a significant error.[9] In this work we have therefore employed an approximate size correction

factor derived from the measurements of Aerts (see Supporting Information Figure S5).[9] This provided a rough initial estimate of the particle diameter, which was then confirmed to be reasonable by comparison with the DLS data. As **II** was observed only at very low Q and continued beyond the range of the detector, its intensity was measured using a single-point analysis as close to $Q = 0$ as possible. An invariant-type analysis (Supporting Information Figure S6) of the SAXS patterns was also performed to estimate the total volume of scattering material (i.e., species large enough to be within the limits of the SAXS detector range).

The amount of crystalline material was determined using the normalized area of the (622) Bragg reflection from the WAXS data fitted using the XFIT software suite, and the amount at the end of the reaction was then used to define the extent of reaction (α).[46] To obtain additional information about this crystallization process, Avarami and "Sharp−Hancock" analyses (Supporting Information Figure S7), similar to those performed on other microporous materials, were also performed on the crystallization curves.[47−53] Generally these analyses were performed between $\alpha = 0.15$ and $\alpha = 0.8$, as deviations during the very early and late parts of crystallization have been known to affect the results. However, as discussed below, a second growth stage between $\alpha = 0.84$ and $\alpha = 0.96$ was also identified in the unsubstituted system, and a separate analysis was therefore performed on this part of the data.

In Situ Dynamic Light Scattering. ***Experimental Setup.*** Prior to performance of the DLS measurements, the viscosity of the unsubstituted zeolite solution at 90 °C was measured as a function of time using an Anton Paar Physica MCR300 shear rheometer (Supporting Information Figure S8). The variation of viscosity with time was used to correct the particle size obtained from the DLS curves.[30] In situ DLS experiments were performed on a Malvern Instruments Zetasizer Nano device with a size range of 0.6 nm to 6 μm. As with the SAXS experiments, the sample holder was heated to 90 °C, the cell (in this case a glass cuvette) was inserted into the system preheated to this temperature, and the measurement was started; measurements were performed approximately every 3 min. For this experiment the sample cuvette had a maximum volume of 1.5−3 mL, slightly larger than that of the SAXS cell. This, combined with the different experimental geometries and thermal convection conditions, resulted in a significant variation in the overall rate at which crystallization occurred (i.e., the process was slower in the DLS setup). This must then be taken into account when the SAXS and DLS results are compared.

Data Analysis. The particle size distribution by intensity from DLS, taking into account our viscosity measurements, is derived from a deconvolution of the measured intensity autocorrelation function of the sample. This deconvolution was performed using a non-negatively constrained least-squares (NNLS) fitting algorithm of the Malvern Dispersion Technology Software, version 5.10. The obtained apparent size is an equivalent sphere diameter.

Results and Discussion

Ex Situ Phase Analysis. The successful synthesis of Ge-substituted zeolite A was confirmed using ex situ tests on the final experimental products. Figure 1 demonstrates the formation of the phase-pure LTA by XRD. Some shifts in the peak positions (particularly at high 2θ) were noted at high Ge substitution levels, indicating the expected expansion of the unit cell due to Ge insertion into the crystalline framework. This was quantified by Le Bail fits, revealing an expansion of the unit cell parameters and increase in cell volume (Table 1).[54−56] An EXAFS analysis of the first shell also supports isomorphous substitution, giving tetrahedral Ge coordination ($N = 3.7 \pm 0.4$) with bond distances (Ge−O) of 1.719 ± 0.02 Å (similar to Ge^{4+} substitution in other zeolitic systems).[57] EDX analysis revealed that the level of substitution was approximately as expected, with concentrations of 8.0%, 12.9%, and 25.5% for the 5%, 10%, and 23% substituted samples, respectively, which are within error for unpolished samples.

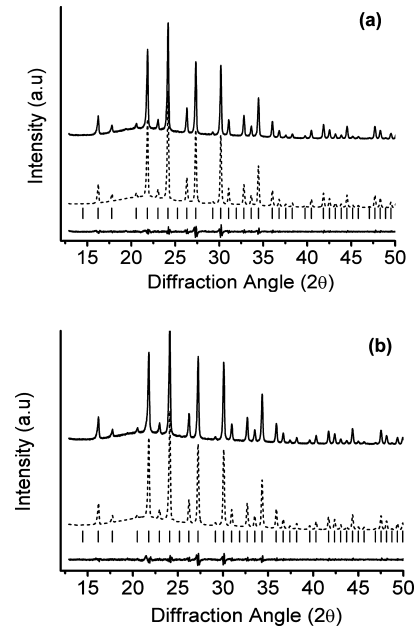

Figure 1. Le Bail fits for unsubstituted (a) and 23% substituted (b) zeolite A. The observed (solid, top), calculated (dashed), and difference (solid, bottom) lines are given as well as the Bragg peak positions (ticks).

TABLE 1: Results of the Le Bail Fit of the Unsubstituted and 23% Substituted Zeolite A

parameter	0%	23%
$a = b = c$ (Å)	12.20052(12)	12.24187(12)
volume (Å^3)	1816.08(3)	1834.61(3)
R_p	2.76	2.79
R_{wp}	3.76	3.72
R_{exptl}	2.02	2.16
χ^2	3.27	2.97

This ex situ data therefore indicates that a high proportion of Ge was successfully incorporated into the zeolite A framework in a manner similar to that observed for the silicalite-1 system.[11]

Initial Analysis. Initially we discuss the unsubstituted system to determine the particles present and the overall formation mechanism. Figure 2 represents an overview of the entire formation process observed by SAXS/WAXS, DLS, and SEM. It plots measurements that cover the entire length scale of the formation process from the nanoscale to the final submicrometer crystalline products. From the selected SAXS plots (Figure 2a,b) and DLS contour data (Figure 2c), we observe the formation of three distinct particle populations (**I**, **II**, and **III**) of increasing size, with **II** forming as the number density of **I** decreases and **III** forming much later in the reaction. A more detailed comparison of the data obtained from the SAXS/WAXS measurements (as detailed in the Supporting Information) then gives additional information on particles **I** and **II** in relation to the observation of Bragg crystalline materials (Figure 2d). The

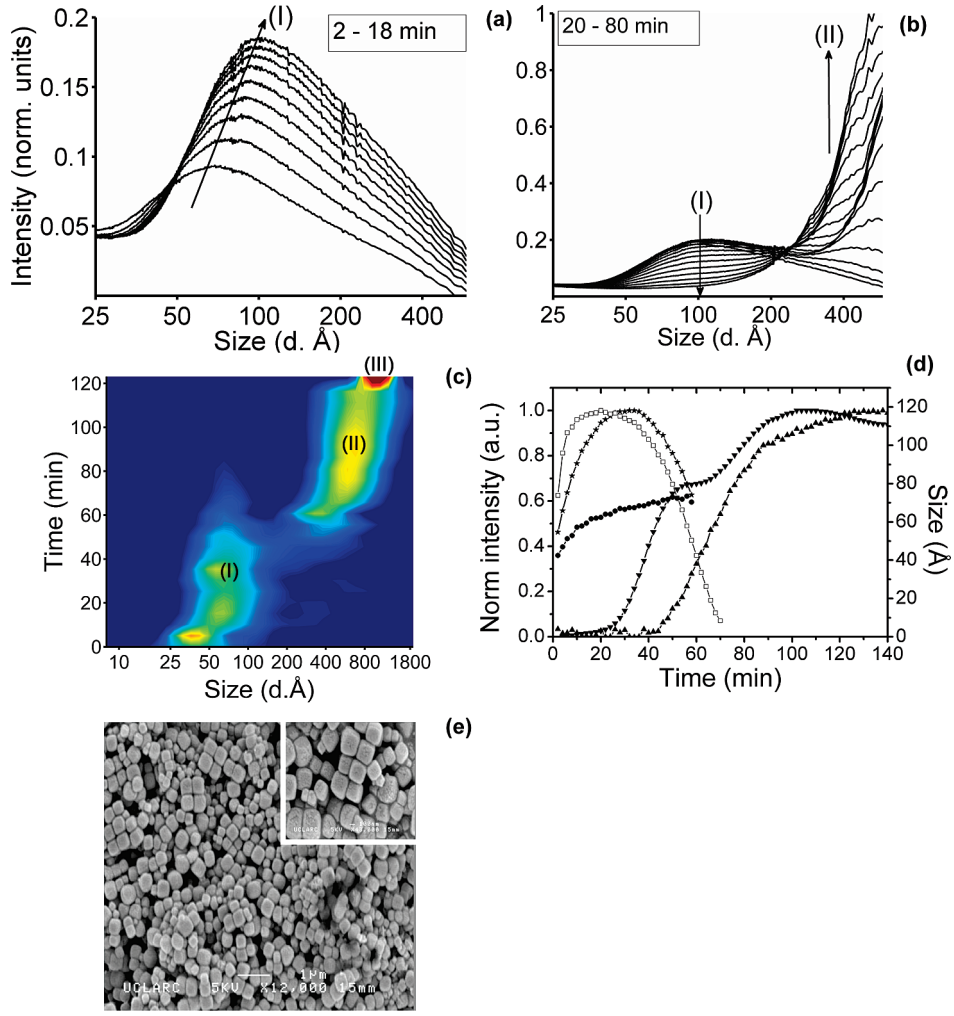

Figure 2. Selected SAXS plots from an unsubstituted zeolite A solution at 90 °C showing an initial increase in scattering intensity and diameter of nanoparticles **I** (a), followed by a subsequent decrease in intensity as aggregates **II** were formed (b). A time-resolved DLS contour plot also revealed these features and a narrowing of the PSD of **III** later in the reaction (c). For comparison a number of characteristics of the SAXS data, including the maximum intensity (★) and diameter (●) of nanoparticles **I**, the invariant measurement of the system (□), the intensity of aggregates **II** (▼), and the formation of Bragg crystallites as measured by WAXS (▲) are given in (d). An SEM image of the final crystalline product is then demonstrated (e).

similarity between the increase in the number density of **II** and the growth of crystallites then suggests that these features are related and that **II** obtains a crystalline character as the reaction proceeds. Finally, Figure 2e reveals the morphology of the final cubic crystalline product as detailed by SEM.

The corrected modal size (see the Experimental Section and Supporting Information Figure S5 for details) of **I** derived from the SAXS data varied from ∼42 to ∼72 Å until unobservable due to a decreased scattering intensity. This compares well with that from DLS (from ∼40 to 75 Å), demonstrating that the correction factor used is reasonable.[9] As **II** was only partially within the SAXS camera range, its size was determined from DLS alone, the modal size distribution being initially ∼300 Å, which then increased to ∼780 Å. **III** was then larger (∼1000 Å) and had a much narrower particle size distribution (PSD) compared to **II**, due primarily to "consumption" of the smaller particles making up **II**. The PSD of **III** at the end of the experiment varied from 580 to 1700 Å, which was broadly similar to that observed by SEM. Some larger particles were observed by SEM; however, these are likely a consequence of the different synthesis times between the experiments (2 h for DLS and 3 h for SEM) and the aforementioned differences in reactor vessel size, geometry, and thermal conditions.

Formation Mechanism. The formation mechanism of this unsubstituted zeolite A solution appears to be broadly similar to that deduced by the group of Tsapatsis and co-workers for the aggregate-based formation of silicalite-1 from nanoparticles that play an active role in the synthesis.[21,58,59] Nanoparticles **I** were observed from the very initial SAXS scan (2 min). However, a comparison with a SAXS measurement at room temperature after 2 min (Supporting Information Figure S9) indicates that, unlike the silicalite-1 synthesis,[21,58,59] these particles were not spontaneously formed on mixing of the gel, but required heating to reaction temperatures. This indicates that nanoparticle formation in this system is slower than in silicalite-1 at room temperature. We also find no evidence for smaller "primary"-type particles as observed in some previous studies, suggesting that these nanoparticles are formed by a solution species mediated transport mechanism.[14,28] This is supported by the very rapid increase in the amount of scattering material observed by the SAXS camera (invariant-type analysis) during the first few moments of the experiment, which coincided with the most rapid increase in size and scattering intensity of nanoparticles **I**.

After this period of rapid change, nanoparticles **I** increased only slowly in size as initial "aging" occurred. This then

continued until the second larger distribution of particles **II** was observed (at ~20−24 min). Thereafter, no further size change of **I** occurred, although the scattering intensity did decrease as **II** continued to grow, as observed in a number of SAXS studies.[14,24] Thus, this stage then represents the evolution of the nanoparticles to the point at which they have become significantly organized to form the larger aggregates **II**, which then grow by addition of the nanoparticles to the growing surface.[59] Interestingly, however, we note no evidence of an extended period during which the nanoparticles underwent a stability increase without a further size increase.[47] This could be a simple consequence of the higher temperature and more rapid formation mechanism in this experiment compared to the silicalite-1 works, however, it could also indicate that the nanoparticles here were less zeolite-like when they aggregated. Such a hypothesis then fits well with the recent modification of the silicalite-1 mechanism where the initial aggregates are now considered to have a "not well developed structure", rather than an organized zeolite-like structure.[58] A comparison of the appearance of aggregates **II** in SAXS with the observation of Bragg crystallites by WAXS in our system supports this suggestion, with an observed difference of 20 min between the two events. Of course, we note that WAXS is known to be less sensitive to very small amounts of crystalline materials compared to SAXS. However, such a large time difference between the two observations suggests that aggregates **II** are initially highly disordered and only with time develop Bragg crystallinity.

Growth of these larger aggregates then continued by addition of the nanoparticles to the growing surface, with increasing internal organization from the not well developed state to the final crystalline zeolite state. While the exact nature of this organization stage cannot be determined from this study, we note that previous TEM studies on zeolite A type solutions have revealed the formation of crystalline domains within large globally disordered particles, and such a process may therefore be occurring here.[26]

Finally, we note the observed narrowing of the PSD of aggregates **II** to form the third distribution of particles **III**. The occurrence of this process at such a late stage in the DLS experiment indicates that, despite the aforementioned difference in rates of reaction, Bragg crystallization was well under way. Combined with the fact that particles **III** were very similar in size to the final crystals as observed by SEM, it is reasonable to suggest that particles **III** represent the final stages of zeolite A formation. Further, as the PSD narrowing was entirely at the expense of the lower part of the distribution of **II**, this stage then represents a final "Ostwald-like ripening" of the crystallites. Such a process most likely occurs by the attachment of the smaller crystallites to form larger ones, similarly to the attachment of the nanoparticles earlier in the reaction, or by the dissolution and transport of the smaller crystallites over extended periods in solution. However, we note that addition of some remaining **I** or small oligomers, below the size and number density detection limit of the detectors used in these experiments, could also occur.

From these data, we present in Figure 3 a schematic representation of a suggested formation mechanism of a zeolite A from this clear solution. It is broadly similar to the modified mechanism proposed by Tsapatsis (for silicate-1) and includes the solution-mediated formation of the initial nanoparticles, which then become larger and more ordered and convert to the initially globally disordered aggregates that then grow by continued nanoparticle addition.[21,58,59] These aggregates then convert by some mechanism to the crystalline zeolite materials

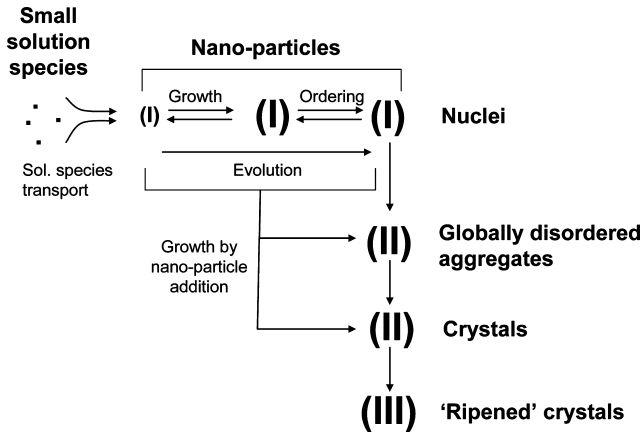

Figure 3. Schematic of the growth mechanism of unsubstituted zeolite A which is broadly similar to that observed previously for silicalite-1 where **I**, **II**, and **III** represent the three species observed in Figure 2: nanoparticles, aggregates/crystallites, and then ripened crystallites, respectively.

which continue to grow and then undergo a ripening process at a later stage to form the final observed products.

Effect of Ge. We now discuss the effect of Ge substitution on this formation process—from the observed nanoparticles to the aggregates and the final crystallites. For maximum contrast, we concentrate on a 23% substituted system, although measurements from 5% and 10% substituted systems are also included when required to clarify the trends.

Figure 4 presents the same information as Figure 2, but for the 23% substituted system, although the SAXS data were recorded at a shorter camera length, making the observation of **II** more difficult. It is immediately apparent that the overall formation process remained broadly similar to that of the unsubstituted system, but that the rates at which the changes occur were considerably accelerated. As described in the Introduction, this effect is well-known and has been attributed to the stabilization of particular structures such as D4 rings and acute angles required to synthesize zeolites.[35−40] The generality of this effect was then confirmed by observing the rate of change as a function of Ge substitution, with Figure 5 and Table 2 detailing the crystallization curves, induction times, and calculated rates of reaction as derived from a Sharp−Hancock and Avrami analysis (see Supporting Information Figure S7).[48,60] The data reveal that the enhancement effect of Ge was generally proportional to the increase in substitution level, although there was little effect at low substitution levels (cf. 0% and 5%). As expected, the "dimensionalities" of each experiment were also identical, indicating a similar crystal growth process in each case.[61]

While enhancement effects of Ge are not new, the combination of in situ and ex situ data and the ability to compare unsubstituted and substituted systems now allows us to gain more detail into both the nature of the entire formation process and the role of Ge therein. Indeed, from the very beginning of the reaction, it is clear that Ge had a significant effect, resulting in larger nanoparticles **I**, as is clearly demonstrated in Figure 6a with an overlay of a SAXS scan from the unsubstituted and 23% substituted samples after 2 min of heating. Measurement of the modal PSD of the nanoparticles throughout the reaction at the various substitution levels (Figure 6b) reveals how this increase in size is proportional to the Ge substitution level, indicating a clear stabilization effect of Ge with regard to larger nanoparticles.

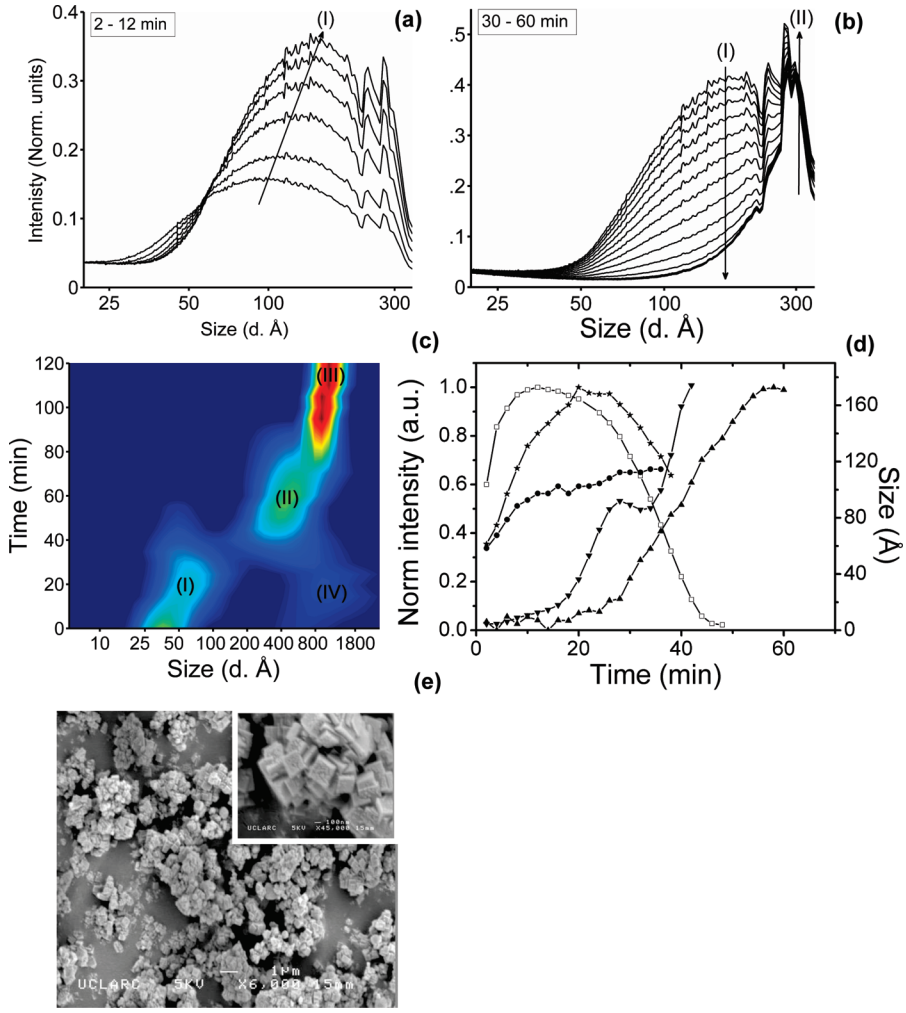

Figure 4. Selected SAXS plots from a 23% substituted zeolite A at 90 °C show features identical to those of the unsubstituted system (a, b). The three expected features were also observed in the corresponding DLS contour plot; however, an additional larger species was also observed in small quantities (**IV**) during the initial stages of growth (c). A plot of the various SAXS features (key as in Figure 2) demonstrates that they follow a similar pattern, albeit at a faster rate of change (d), while the SEM image of the final materials revealed morphological changes to the final product (e).

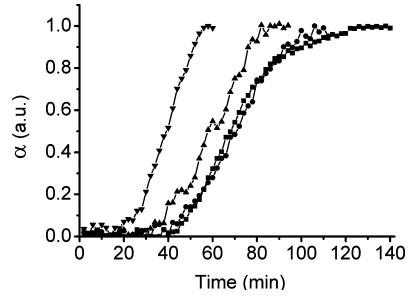

Figure 5. Growth of the zeolite crystals (from the WAXS data) for unsubstituted (■) and 5% (●), 10% (▲), and 23% (▼) substituted samples.

TABLE 2: Results from the Sharp−Hancock Analysis for Each of the Crystallization Curves, Giving the Induction Time, Rate of Reaction (k), and Dimensionality (n)

sample	α region	induction time (min)	k (min^{-1})	n
0%	0.15−0.85	42	0.033(3)	1.6(1)
5%	0.15−0.85	42	0.029(3)	1.6(1)
10%	0.15−0.85	34	0.032(3)	1.7(1)
23%	0.15−0.85	24	0.049(4)	1.6(1)

Furthermore, the directly proportional relationship between the increased stability of nanoparticles on Ge substitution and the increase in crystallization rate supports the importance of the nanoparticles in the growth process. This can be understood by considering that, if the formed nanoparticles were acting only as nutrient sources for a monomeric formation mechanism, then their dissolution would most likely represent a rate-limiting step with regard to the rate of crystallization. Any stabilization of these nanoparticles (for example, by Ge-induced local pH rises or salting out) would then result in decreased dissolution and crystallization rates, i.e., an inverse stability-crystallization relationship and not the direct relationship observed here.[11,28] Additionally, we note that Ge substitution actually has little effect on the pH of the various gels (pH 13.8 ± 0.1), making salting out unlikely.[28]

Considering these observations with regard to the proposed mechanism, it therefore seems likely that Ge has a fundamentally important effect on the entire formation process and that the Ge-substituted nanoparticles are directly involved in this process.

The exact manner in which Ge stabilizes the forming nanoparticles (and later the crystalline material) is more difficult to assess from the data available. However, the stabilization occurred very early in the reaction and led to a more rapid

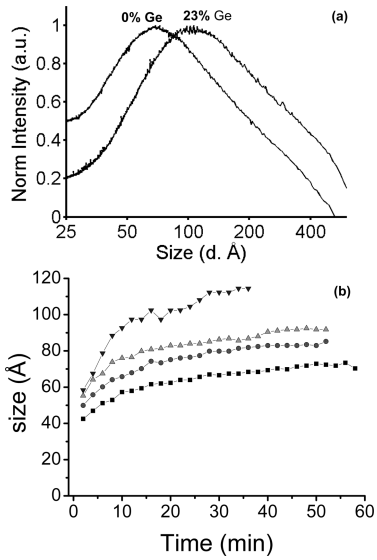

Figure 6. SAXS plots of **I** from the unsubstituted and 23% substituted data both after 2 min of reaction (a) and the average size of the aggregate particles of the 0% (■), 5% (●), 10% (▲), and 23% (▼) substituted samples as a function of time (b).

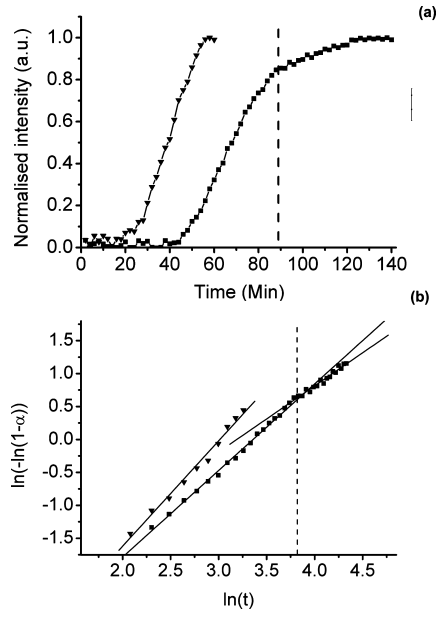

Figure 7. Comparison of the unsubstituted (■) and 23% subsituted (▼) crystallization curves (a) and resulting linear fits from a Sharp−Hancock analysis (b). The dashed line indicates the point of inflection in both panels.

formation of the growing aggregates and the final framework, in which the Ge was incorporated. Therefore, while we can present no direct evidence for the formation of specific important "zeolite building blocks", from the evidence of previous works and the mechanism presented, it seems reasonable to suggest that inclusion of Ge allows more rapid formation of stabilized zeolite-like building blocks early in the reaction, allowing the ordering of the zeolite framework to occur more quickly.[21,28,36,41]

Aside from the early part of the growth process, Ge also had a significant effect on the crystallization stage of the process. For example, in Figure 7, detailed crystallization curves for the unsubstituted and 23% substituted systems along with corresponding logarithmic Sharp−Hancock plots are given. A distinct

TABLE 3: Comparison of the Sharp−Hancock Data for the Two Parts of the Unsubstituted System[a]

sample	α region	induction time (min)	k (min^{-1})	n
0%	0.15−0.85	42	0.033(3)	1.6(1)
0%	0.84−0.96	n/a	0.008(1)	1.4(1)

[a] Definitions as in Table 2.

inflection point is observed but only in the unsubstituted system after ∼88 min (extent of reaction α = 0.84). Such a feature is similar to the "pauses" observed in previous crystallization studies and indicates a change in the crystallization process.[51,62] This is confirmed in Table 3 where we find that both the rate of reaction (from 0.049 to 0.008 min^{-1}) and the dimensionality (from 1.6 to 1.4) decrease after the inflection point (α = 0.84 and 0.96). This then demonstrates how metal substitution can not only affect the early stages of a zeolite formation process (i.e., the formation of nanoparticles and the rate of conversion to aggregates/crystallites), but also the latter stages of crystallization, here giving rise to a two-stage, rather than a single-stage, process. The reason for such an effect remains under investigation, although we note an intriguing link between the projected complete consumption of nanoparticles and the observed inflection point (Supporting Information Figure S10). Of course, such a link is at this stage only tentative as the scattering intensities of SAXS and WAXS are not directly comparable. However, as the initial nanoparticles contain the Ge that is incorporated into the final product, it seems reasonable to propose a link between the consumption of these nanoparticles and the changes in the final crystallization process.

Such changes in the formation process should also manifest themselves in the final zeolite products, and indeed, if we compare the SEM images for the two systems (Figures 2e and 4e), a significant change in morphology is clear. For the unsubstituted system the crystals were found to be well-defined cubes with rounded edges and corners, while in the substituted system they have become significantly intergrown but have much "sharper" and more defined edges and corners on the individual crystals. Such morphological changes are likely to have some effect on the physicochemical properties of the crystals, therefore demonstrating how Ge substitution affects the entire crystallization process and could maybe be used for a more "rational" design and control the final product.

Finally, we note an additional large (500−2000 Å), but weakly scattering, particle population (**IV**) observed by DLS only in the substituted system (Figure 3c). Although the nature of these particles remains under investigation, we note that, unlike the stabilized nanoparticles, this distribution tends to "dissolve" into the forming aggregates **II**. Therefore, while Ge substitution instigates their formation, particles **IV** probably do not consist of any "zeolite-type structure" and are not directly involved in the formation process. Indeed, although the overall effect of Ge on the pH of the solutions was minimal (see above), it is possible that a local, Ge-induced pH precipitation or "salting out" of disorganized Si and Al species can occur alongside the formation of more organized nanoparticles[11,28] Particles **IV** would then act as "nutrient"-type species, breaking down as the zeolite material continues to form.

Conclusions

We have, for the first time, successfully incorporated large amounts of Ge into the framework of zeolite A in a clear

solution environment as demonstrated by ex situ techniques. In situ, time-resolved SAXS/WAXS and DLS studies on an initially unsubstituted system then allowed us to identify a number of precrystalline and crystalline particles (**I**, **II**, and **III**) during the formation process. These particles are similar to those observed in previous studies and indicate an aggregation mechanism that is broadly similar to that observed recently for silicalite-1, where the forming nanoparticles become more stabilized and "zeolite-like" until they convert to initially disordered aggregates which continue to grow and order to form the final zeolite structure.

By then comparing experiments with and without Ge substitution, we have been able to provide further evidence for the important role of the nanoparticles in the zeolite formation. We have also demonstrated how metal framework substituents can affect the entire formation process, from the initially formed nanoparticles to the final crystalline products. Although not directly observed, it seems that Ge stabilization of particular structures (possibly, as seen elsewhere, D4Rs)[28,35−40] within the nanoparticles stabilizes larger particles which then convert to growing aggregates and then the final crystalline material more quickly. Finally, examination of the later stages of the reaction has demonstrated the significant effect of Ge on both the crystal growth process and final morphology.

This work has therefore demonstrated direct in situ evidence for the effect of metal substitution on all parts of the zeolite synthesis process and shown how control of the substitution can not only change the rate of material formation but also alter the nature of the final product. Understanding metal substitution effects is therefore essential if the rational design of more morphologically functional porous materials is to be achieved.

Acknowledgment. We thank the EPSRC and NWO-CW (Veni) for funding, Emile Bakelaar for rheology measurements, and Chris Martin (formerly station 6.2 SRS, Daresbury) and Wim Bras for useful discussions.

Supporting Information Available: EXAFS data, 3D SAXS plots, detector response corrections, the experimental cell, SAXS size correction, invariant type analysis, Avarami/Sharp−Hancock analysis, viscosity measurements, room temperature measurements, and a possible relationship between aggregate consumption and crystal growth. This material is available free of charge via the Internet at http://pubs.acs.org.

References and Notes

(1) Rouquerol, J.; Avnir, D.; Fairbridge, C. W.; Everett, D. H.; Haynes, J. H.; Pernicone, N.; Ramsay, J. D. F.; Sing, K. S. W.; Unger, K. K. *Pure Appl. Chem.* **1994**, *66*, 1739.

(2) Stocker, M. *Microporous Mesoporous Mater.* **1999**, *29*, 3.

(3) Doronin, V. P.; Sorokina, T. P. *Russ. J. Gen. Chem.* **2007**, *77*, 2224.

(4) Khadzhiev, S. N.; Kolesnichenko, N. V.; Ezhova, N. N. *Pet. Chem.* **2008**, *48*, 325.

(5) Lobo, R. *AIChE J.* **2008**, *54*, 1402.

(6) Lewis, D. W.; Willock, D. J.; Catlow, C. R. A.; Thomas, J. M.; Hutchings, G. J. *Nature* **1996**, *382*, 604.

(7) Cundy, C. S.; Cox, P. A. *Chem. Rev.* **2003**, *103*, 663.

(8) Cundy, C. S.; Cox, P. A. *Microporous Mesoporous Mater.* **2005**, *82*, 1.

(9) Aerts, A.; Follens, L. R. A.; Haouas, M.; Caremans, T. P.; Delsuc, M. A.; Loppinet, B.; Vermant, J.; Goderis, B.; Taulelle, F.; Martens, J. A.; Kirschhock, C. E. A. *Chem. Mater.* **2007**, *19*, 3448.

(10) Cheng, C. H.; Juttu, G.; Mitchell, S. F.; Shantz, D. F. *J. Phys. Chem. B* **2006**, *110*, 22488.

(11) Cheng, C. H.; Juttu, G.; Mitchell, S. F.; Shantz, D. F. *J. Phys. Chem. B* **2006**, *110*, 21430.

(12) de Moor, P.; Beelen, T. P. M.; van Santen, R. A.; Beck, L. W.; Davis, M. E. *J. Phys. Chem. B* **2000**, *104*, 7600.

(13) de Moor, P.; Beelen, T. P. M.; van Santen, R. A. *Microporous Mater.* **1997**, *9*, 117.

(14) de Moor, P.; Beelen, T. P. M.; van Santen, R. A. *J. Phys. Chem. B* **1999**, *103*, 1639.

(15) Schoeman, B. J.; Sterte, J.; Otterstedt, J. E. *Zeolites* **1994**, *14*, 208.

(16) Persson, A. E.; Schoeman, B. J.; Sterte, J.; Ottesstedt, J. E. *Zeolites* **1994**, *14*, 557.

(17) Twomey, T. A. M.; Mackay, M.; Kuipers, H.; Thompson, R. W. *Zeolites* **1994**, *14*, 162.

(18) Schoeman, B. J. *Zeolites* **1997**, *18*, 97.

(19) Singh, P. S.; Dowling, T. L.; Watson, J. N.; White, J. W. *Phys. Chem. Chem. Phys.* **1999**, *1*, 4125.

(20) Smaihi, M.; Barida, O.; Valtchev, V. *Eur. J. Inorg. Chem.* **2003**, 4370.

(21) Davis, T. M.; Drews, T. O.; Ramanan, H.; He, C.; Dong, J. S.; Schnablegger, H.; Katsoulakis, M. A.; Kokkoli, E.; McCormick, A. V.; Penn, R. L.; Tsapatsis, M. *Nat. Mater.* **2006**, *5*, 400.

(22) Liang, D.; Follens, L. R. A.; Aerts, A.; Martens, J. A.; Van Tendeloo, G.; Kirschhock, C. E. A. *J. Phys. Chem. C* **2007**, *111*, 14283.

(23) Schoeman, B. J. *Microporous Mesoporous Mater.* **1998**, *22*, 9.

(24) de Moor, P.; Beelen, T. P. M.; Komanschek, B. U.; Beck, L. W.; Wagner, P.; Davis, M. E.; van Santen, R. A. *Chem.—Eur. J.* **1999**, *5*, 2083.

(25) Grizzetti, R.; Artioli, G. *Microporous Mesoporous Mater.* **2002**, *54*, 105.

(26) Mintova, S.; Olson, N. H.; Valtchev, V.; Bein, T. *Science* **1999**, *283*, 958.

(27) Nikolakis, V.; Kokkoli, E.; Tirrell, M.; Tsapatsis, M.; Vlachos, D. G. *Chem. Mater.* **2000**, *12*, 845.

(28) Fan, W.; Ogura, M.; Sankar, G.; Okubo, T. *Chem. Mater.* **2007**, *19*, 1906.

(29) Kirschhock, C. E. A.; Buschmann, V.; Kremer, S.; Ravishankar, R.; Houssin, C. J. Y.; Mojet, B. L.; van Santen, R. A.; Grobet, P. J.; Jacobs, P. A.; Martens, J. A. *Angew. Chem., Int. Ed.* **2001**, *40*, 2637.

(30) Kirschhock, C. E. A.; Kremer, S. P. B.; Vermant, J.; Van Tendeloo, G.; Jacobs, P. A.; Martens, J. A. *Chem.—Eur. J.* **2005**, *11*, 4306.

(31) Bu, X. H.; Feng, P. Y.; Stucky, G. D. *Science* **1997**, *278*, 2080.

(32) O'Brien, M. G.; Beale, A. M.; Catlow, C. R. A.; Weckhuysen, B. M. *J. Am. Chem. Soc.* **2006**, *128*, 11744.

(33) Paillaud, J. L.; Harbuzaru, B.; Patarin, J.; Bats, N. *Science* **2004**, *304*, 990.

(34) Warrender, S. J.; Wright, P. A.; Zhou, W. Z.; Lightfoot, P.; Camblor, M. A.; Shin, C. H.; Kim, D. J.; Hong, S. B. *Chem. Mater.* **2005**, *17*, 1272.

(35) Blasco, T.; Corma, A.; Diaz-Cabanas, M. J.; Rey, F.; Vidal-Moya, J. A.; Zicovich-Wilson, C. M. *J. Phys. Chem. B* **2002**, *106*, 2634.

(36) Kamakoti, P.; Barckholtz, T. A. *J. Phys. Chem. C* **2007**, *111*, 3575.

(37) Meza, L. I.; Anderson, M. W.; Agger, J. R. *Chem. Commun.* **2007**, 2473.

(38) O'Keeffe, M.; Yaghi, O. M. *Chem.—Eur. J.* **1999**, *5*, 2796.

(39) Rimer, J. D.; Roth, D. D.; Vlachos, D. G.; Lobo, R. F. *Langmuir* **2007**, *23*, 2784.

(40) Sastre, G.; Pulido, A.; Castaneda, R.; Corma, A. *J. Phys. Chem. B* **2004**, *108*, 8830.

(41) Schaack, B. B.; Schrader, W.; Schuth, F. *Chem.—Eur. J.* **2009**, *15*, 5920.

(42) Mintova, S.; Fieres, B.; Bein, T. *Impact of Zeolites and Other Porous Materials on the New Technologies at the Beginning of the New Millennium, Pts a and b*; Elsevier Science: Amsterdam, 2002; Vol. 142, p 223.

(43) Cernik, R. J.; Barnes, P.; Bushnell-Wye, G.; Dent, A. J.; Diakun, G. P.; Flaherty, J. V.; Greaves, G. N.; Heeley, E. L.; Helsby, W.; Jacques, S. D. M.; Kay, J.; Rayment, T.; Ryan, A.; Tang, C. C.; Terrill, N. J. *J. Synchrotron Radiat.* **2004**, *11*, 163.

(44) Koch, M. OTOKO (modified from XOTOKO).

(45) Glatter, O.; Kratky, O. *Small Angle X-ray Scattering*; Academic Press: London, 1982.

(46) Coelho, A. A.; Cheary, R. W. X-ray Line Profile Fitting Program (XFIT), version 0.07.002, 1997.

(47) Davies, A. T.; Sankar, G.; Catlow, C. R. A.; Clark, S. M. *J. Phys. Chem. B* **1997**, *101*, 10115.

(48) Hancock, J. H.; Sharp, J. D. *J. Am. Ceram. Soc.* **1972**, *55*, 74.

(49) Norby, P.; Christensen, A. N.; Hanson, J. C. *Inorg. Chem.* **1999**, *38*, 1216.

(50) O'Brien, M. G.; Sanchez-Sanchez, M.; Beale, A. M.; Lewis, D. W.; Sankar, G.; Catlow, C. R. A. *J. Phys. Chem. C* **2007**, *111*, 16951.

(51) Walton, R. I.; Millange, F.; O'Hare, D.; Davies, A. T.; Sankar, G.; Catlow, C. R. A. *J. Phys. Chem. B* **2001**, *105*, 83.

(52) Beale, A. M.; Sankar, G. *Chem. Mater.* **2003**, *15*, 146.

(53) Fogg, A. M.; Price, S. J.; Francis, R. J.; O'Brien, S.; O'Hare, D. *J. Mater. Chem.* **2000**, *10*, 2355.

(54) Dwyer, J.; Dewing, J.; Karim, K.; Holmes, A. J.; Ojo, A. F.; Garforth, A. A.; Rawlence, D. J. In *Proceedings of the International Symposium*, Prague; Jacobs, P. A., Jaeger, N. I., Kubelkova, L., Wichterlova, B., Eds.; Elsevier: Amsterdam, 1991; p 1.
(55) Dwyer, J.; Karim, K. *J. Chem. Soc., Chem. Commun.* **1991**, 905.
(56) Flanigen, E. M.; Grose, R. W. In *Advances in Chemistry Series*; Van Bekkum, H., Flanigen, E. M., Jansen, J. C., Eds.; American Chemical Society: Washington, DC, 1971; Vol. 101, p 76.
(57) Tuilier, M. H.; Lopez, A.; Guth, J. L.; Kessler, H. *Zeolites* **1991**, *11*, 662.
(58) Kumar, S.; Wang, Z. P.; Penn, R. L.; Tsapatsis, M. *J. Am. Chem. Soc.* **2008**, *130*, 17284.
(59) Kumar, S.; Davis, T. M.; Ramanan, H.; Penn, R. L.; Tsapatsis, M. *J. Phys. Chem. B* **2007**, *111*, 3398.
(60) Avarami, M. *J. Chem. Phys.* **1941**, *9*, 177.
(61) Hulbert, S. F. *J. Br. Ceram. Soc.* **1969**, *6*, 11.
(62) Millange, F.; Walton, R. I.; O'Hare, D. *J. Mater. Chem.* **2000**, *10*, 1713.

JP907542A